Structure and Spectroscopy of the Periplasmic Cytochrome *c* Nitrite Reductase from *Escherichia coli*†

Vicki A. Bamford,‡ Hayley C. Angove,‡ Harriet E. Seward,§ Andrew J. Thomson,§ Jeffrey A. Cole,⊥ Julea N. Butt,§,‡ Andrew M. Hemmings,*,§,‡ and David J. Richardson*,‡

Centre for Metalloprotein Spectroscopy and Biology, School of Biological Sciences, and School of Chemical Sciences, University of East Anglia, Norwich, NR4 7TJ, United Kingdom, and School of Biosciences, University of Birmingham, Edgbaston, Birmingham B15 2TT, United Kingdom

Received September 11, 2001; Revised Manuscript Received December 20, 2001

ABSTRACT: The crystal structure and spectroscopic properties of the periplasmic penta-heme cytochrome *c* nitrite reductase (NrfA) of *Escherichia coli* are presented. The structure is the first for a member of the NrfA subgroup that utilize a soluble penta-heme cytochrome, NrfB, as a redox partner. Comparison to the structures of *Wolinella succinogenes* NrfA and *Sulfospirillum deleyianum* NrfA, which accept electrons from a membrane-anchored tetra-heme cytochrome (NrfH), reveals notable differences in the protein surface around heme 2, which may be the docking site for the redox partner. The structure shows that four of the NrfA hemes (hemes 2−5) have bis-histidine axial heme-Fe ligation. The catalytic heme-Fe (heme 1) has a lysine distal ligand and an oxygen atom proximal ligand. Analysis of NrfA in solution by magnetic circular dichroism (MCD) suggested that the oxygen ligand arose from water. Electron paramagnetic resonance (EPR) spectra were collected from electrochemically poised NrfA samples. Broad perpendicular mode signals at $g \sim 10.8$ and 3.5, characteristic of weakly spin-coupled $S = 5/2$, $S = 1/2$ paramagnets, titrated with $E_m = -107$ mV. A possible origin for these are the active site Lys-OH_2 coordinated heme (heme 1) and a nearby bis-His coordinated heme (heme 3). A rhombic heme Fe(III) EPR signal at $g_z = 2.91$, $g_y = 2.3$, $g_x = 1.5$ titrated with $E_m = -37$ mV and is likely to arise from bis-His coordinated heme (heme 2) in which the interplanar angle of the imidazole rings is 21.2°. The final two bis-His coordinated hemes (hemes 4 and 5) have imidazole interplanar angles of 64.4° and 71.8°. Either, or both, of these hemes could give rise to a "Large g max" EPR signal at $g_z = 3.17$ that titrated at potentials between −250 and −400 mV. Previous spectroscopic studies on NrfA from a number of bacterial species are considered in the light of the structure-based spectro-potentiometric analysis presented for the *E. coli* NrfA.

The reduction of nitrate to ammonium in the periplasm of *Escherichia coli* involves two enzymes, periplasmic nitrate reductase and periplasmic nitrite reductase (NrfA).[1] The process is found in many enteric bacteria and may be important for anaerobic nitrate and nitrite respiration at low nitrate concentrations (*1*, *2*). The NrfA protein catalyzes the six electron reduction of nitrite to ammonium, but can also catalyze the five electron reduction of NO and two electron reduction of hydroxylamine, both of which may be bound intermediates in the catalyic cycle for nitrite reduction (*3*). Although originally described as a hexa-heme cytochrome (*4*), more recent primary structure and biochemical analysis revealed that the *E. coli* NrfA protein is a 52-kDa pentaheme cytochrome in which four hemes are covalently bound to the conventional motif, CXXCH. The fifth heme is attached to the novel CXXCK motif that is essential for catalysis (*5*, *6*).

The crystal structures of cytochrome *c* nitrite reductase from the sulfur reducing bacterium *Sulfurospirillum deleyianum* and the closely related rumen bacterium *Wolinella succinogenes* have been determined recently (*7*, *8*). These structures confirmed biochemical data on the *E. coli* enzyme, demonstrating that the members of the NrfA family are indeed penta-heme cytochromes. In both structures, NrfA crystallized as a homo-dimer, with the hemes within each monomer closely packed to form arrangements of near-parallel and near-perpendicular heme pairs that have also been observed in the *Nitrosomonas europaea* tetra-heme cytochrome *c*554 and octa-heme hydroxylamine oxidoreductase (*9*, *10*) and tetra-heme periplasmic flavocytochrome *c* fumarate reductases from *Shewanella* species (*11*, *12*). The NrfA active site heme displays a distal lysine ligand and water or sulfate depending on the crystallization conditions

† This work was supported by BBSRC Grants 6/P11528 to D.J.R. and J.A.C., and 83/B11958 to D.J.R. and A.J.T., Wellcome Trust Grant 059531/Z/99/Z to D.J.R., A.M.H., and A.J.T., and a Wellcome Trust Career Development award (050709) to J.N.B.

* To whom correspondence should be addressed at the School of Biological Sciences, University of East Anglia, Norwich, NR4 7TJ, U.K. FAX +44 1603 592250. E-mail: d.richardson@uea.ac.uk, a.hemmings@uea.ac.uk.

‡ School of Biological Sciences, University of East Anglia.

§ School of Chemical Sciences, University of East Anglia.

⊥ School of Biosciences, University of Birmingham.

[1] Abbreviations: EPR, electron paramagnetic resonance; MCD, magnetic circular dichroism; RT, room temperature; LT low temperature; NrfA, cytochrome *c* nitrite reductase; NrfH, membrane-anchored tetra-heme cytochrome; NrfB, periplasmic penta-heme cytochrome; NIR, near infrared; LMCT, ligand−metal charge-transfer band.

10.1021/bi015765d CCC: $22.00
Published on Web 02/05/2002

(*7*, *8*). Spectroscopic data have been published for a number of NrfA enzymes (*13*−*18*). However, much of it predates the crystal structures, and interpretation of many of these data must now be reassessed as it was often based on the assumption that the enzyme bound six hemes. In addition, interpretation of some published spectroscopy is complicated by the fact that it was collected from the NrfA complexed with a "partner" cytochrome (*16*, *18*).

Analysis of the organization of *nrfA* gene clusters from a range of bacteria reveals that they can be divided into two groups. In one group, that includes *W. succinogenes* and *S. deleyianum*, the *nrfA* clusters with an adjacent gene *nrfH* which encodes a membrane-anchored tetra-heme quinol dehydrogenase of the NapC family (*8*, *19*, *20*). In the second group, which includes *E. coli*, the *nrfA* clusters with genes encoding a periplasmic penta-heme cytochrome (*nrfB*), a periplasmic (4 × [4Fe4S]) ferredoxin (*nrfC*), and an integral membrane putative quinol dehydrogenase (*nrfD*) (*3*, *5*). Clearly, electron transfer from quinol to the NrfA in the different groups is distinct. The different protein−protein and cofactor−cofactor interactions implicit in this may be reflected by insertions and deletions in loop regions of the polypeptide chain in the two subgroups that can be identified in primary structure analysis (*8*). In this paper, we present the first X-ray crystal structure of a member of the NrfB-dependent sub-group of NrfA enzymes, the *E. coli* NrfA. The structure has been analyzed in combination with an MCD and spectro-potentiometric EPR characterization of the enzyme. This has allowed the assignment of spectroscopic signals and equilibrium redox potentials to individual hemes in the crystal structure.

EXPERIMENTAL PROCEDURES

Materials. Sodium nitrite was purchased from BDH, hydroxylamine from Sigma, deuterium oxide from Aldrich, and BCA reagent from Pierce. Buffer-electrolyte solutions for voltammetric experiments were prepared with analytical grade water (Fisher, total nitrogen content < 0.1 ppm). Hydroxylamine solutions were prepared immediately prior to use, and the pH was adjusted to 7.0 by the addition of sodium hydroxide.

Growth of Bacteria. The *E. coli* K-12 strain LCB2048 is defective in the nitrate reductases A and Z and expresses the formate-dependent nitrite reductase (NrfA) at elevated levels (*21*). Cultures of strain LCB2048 were grown in minimal salts medium (*21*) without aeration overnight at 37 °C after the addition of kanamycin (25 μg/mL) and spectinomycin (25 μg/mL). Initial cultures (250 mL) were inoculated with 0.5 mL of an overnight culture grown aerobically on Luria-Bertani broth medium. The 250-mL culture was transferred to 2 L of fresh medium and then 6 L of culture was transferred into 100 L of fresh medium.

Activity Assays. Nitrite reductase activity was measured spectrophotometrically by substrate-dependent oxidation of reduced methyl viologen ($\epsilon_{600\ nm}$ = 13 700 M^{-1} cm^{-1}). Assays (3.5 mL final volume) were carried out by mixing at 25 °C in anaerobic cuvettes containing 1 mM methyl viologen, 2 mM $CaCl_2$, 50 mM Hepes, pH 7.0, and either nitrite or hydroxylamine. Methyl viologen was reduced by the addition of sodium dithionite, and turnover was initiated by the addition of NrfA (0.14 μg/mL). Data were fitted to the Michaelis-Menton description of enzyme kinetics to determine K_M for nitrite or hydroxylamine.

Purification of E. coli NrfA. Periplasmic proteins were extracted from the harvested cells as previously described (*21*). NrfA was identified in both the periplasmic and membrane fractions and the distribution between the two fractions varied in different preparations. The enzyme was precipitated from the periplasm using 65% saturated ammonium sulfate and then resuspended in 50 mM Tris-HCl, pH 7.0. NrfA in the membrane fractions was extracted overnight at 4 °C in 50 mM Tris-HCl, pH 7.0, containing 0.1% dodecyl maltoside. The periplasmic or membrane-extracted material was applied to an anion exchange Q-Sepharose column (35 × 3 cm) equilibrated with 50 mM Tris-HCl, pH 7.0. The column was developed using a linear gradient of 0−200 mM NaCl. NrfA eluted at ~80 mM NaCl. The NrfA fraction was applied to a Superdex G-75 Hiload 16/60 FPLC column equilibrated with 50 mM Tris-HCl, pH 7.0. At a flow rate of 1 mL/min and a fraction size of 1 mL, NrfA was eluted in fractions 58−64. NrfA was further purified on an anion exchange Dionex column (0.9 × 25 cm) equilibrated with 50 mM Hepes, pH 7.0, using a SPRINT system. The column was developed using a 0−100 mM NaCl linear gradient, and NrfA eluted at 50 mM NaCl. Protein concentration was determined by the BCA method using bovine serum albumin as a protein standard. The A_{410}/A_{280} ratio was typically 3.5, and the extinction coefficient at 410 nm was 497 650 M^{-1} cm^{-1}, based on a molecular mass of 53 kDa. Periplasmic NrfA was found to run as a single band on native or SDS−polyacrylamide gels either stained with Coomassie blue or for heme. The NrfA prepared from membrane fractions routinely exhibited a 5−10% contamination of iron superoxide dismutase. Aside from that, UV/Visible, EPR and MCD spectroscopy, activity assays, and SELDI analysis established that there were no significant differences between NrfA purified from the periplasmic or membrane fractions, and they were treated as identical after purification. The NrfA used for the crystallography and spectroscopy had a turnover number with nitrite and hydroxylamine of 770 NO_2^- s^{-1} (4600 e^- s^{-1}) and 2380 NH_2OH s^{-1} (4760 e^- s^{-1}) and K_M of 28 μM (NO_2^-) or 30 mM (NH_2OH). The mass of the enzyme determined by SELDI mass spectrometry was 52 997 kDa. Since holo-NrfA binds five hemes each of 615 Da, the predicted mass of the apo-NrfA is 49 922 kDa. NrfA is synthesized with a signal peptide: MTRIKINARRIFSLLIPFFFFTSVHAEQTAAP-**AK**PVTVEAK... (*5*), and the SELDI analysis suggests that the purified NrfA used in this study has been processed at position 33−34 A−K, which yields an apo-protein of 49 925 kDa. In this paper, the amino acid numbering of the unprocessed polypeptide will be used.

Crystal Structure Determination. *E. coli* periplasmic NrfA was concentrated to 10 mg/mL in 50 mM sodium HEPES, pH 7.0, plus 100 mM NaCl. Crystals of typical dimensions 200 × 50 × 10 μm^3 were obtained from vapor diffusion experiments using 20% (w/v) PEG 4000 and 10% (v/v) 2-propanol in 100 mM sodium HEPES buffer at pH 7.5. The crystals could by cryoprotected by transferring them to crystallization solution containing 25% (v/v) glycerol. The crystals belong to space group $P2_12_12_1$ with apparent cell parameters of a = 81.47 Å, b = 90.84 Å, and c = 293.87 Å and contain four molecules of NrfA per asymmetric unit.

X-ray data were collected on station ID14.1 at the ESRF, Grenoble, using a MAR 165 CCD detector and processed to 2.5 Å using DENZO (*22*). The structure of *E. coli* NrfA was solved by molecular replacement using the structure of the homologous enzyme from *S. deleyianum* (PDB accession code 1QDB) as the search model. The program MolRep from the CCP4 program suite (*23*) gave a clear solution for the four molecules with a correlation coefficient of 0.46 and an R_{cryst} of 49.7% in the resolution range of 15.0−4.0 Å. Following rigid body refinement, the R_{cryst} for this model (residues 42−220, 236−246, and 253−495 from the *S. deleyianum* structure) using all data to 2.5 Å had converged to 46.1%.

Model building was carried out using the program O (*24*), and all refinement procedures were performed with CNS (*25*). For refinement, 5% of reflections were set aside for the calculation of R_{free}. Inspection of difference Fourier maps at this stage allowed the manual rebuilding of 382 residues plus the conserved active site calcium ion. The remaining residues, which differ significantly in position between the *S. deleyianum* and *E. coli* structures, were removed from the model. From this point, refinement was performed using a noncrystallographic symmetry restraint of 300 kcal mol^{-1} $Å^{-2}$. A single round of simulated annealing refinement followed by three rounds of conjugate gradient minimization interspersed with manual rebuilding enabled a complete amino acid model to be built for each monomer including all hemes. This process converged to give a R_{cryst} of 24.1% and a R_{free} of 26.0%. After the addition of a second Ca^{2+} ion, a glycerol molecule and 680 water molecules into significant residual electron density the structure refined to give a final R_{cryst} of 20.3% and R_{free} of 24.3%.

The final model consists of residues 38−478, five hemes, two calcium ions, and a glycerol molecule for each of the four molecules in the asymmetric unit plus 680 water molecules. Because of the possibility of reduction during data collection, the oxidation state of the enzyme cannot be clearly established in this structure. When analyzed for stereochemical quality using PROCHECK (*26*) the final structure has all residues in the most favored regions of the Ramachandran plot except His 264 which falls into the generously allowed region in all four molecules. Structural comparisons were carried out using the program DALI (*27*). Representations of molecular electrostatic potential surfaces were prepared using SPOCK (*28*). Coordinates have been deposited in the PDB with the accession code 1GUG.

Spectroscopy. Perpendicular and parallel mode EPR measurements were performed with a Bruker EMX spectrometer equipped with an Oxford ESR-9 liquid helium cryostat and a dual mode cavity with microwave frequencies of 9.65 and 9.35 GHz for the perpendicular and parallel modes, respectively. For EPR of NrfA crystals, around 20 crystals were collected and placed into a reduced volume EPR tube. MCD experiments were recorded on either a circular dichrograph, JASCO J-500, for the wavelength range 280−1000 nm or JASCO J730 for the range 800−2500 nm. Samples were mounted within an Oxford Instruments SM4 split-coil superconducting solenoid capable of generating magnetic fields up to 5 T for low-temperature measurements and in an Oxford Instruments SM1 6 T superconducting solenoid with an ambient temperature bore for room-temperature measurements. Samples were exchanged into deuterated buffer and, for low-temperature MCD measurements, 50% (v/v) glycerol was added as a glassing agent. UV/Vis absorption and EPR spectra of NrfA with or without the glassing agent were identical. For estimating the concentration of hemes from the EPR signals, the following relationship is used (*29*):

$$C = \{(\text{integral of sample}/T_m \text{ of sample})/ (\text{double integral of standard}/T \text{ of standard})\}C_s \quad (1)$$

where C and C_s are the concentration of the heme species and a standard (routinely 1 mM CuEDTA), respectively, and:

$$T = \sqrt{1/3(g_z^2 + g_y^2 + g_x^2)} \quad (2)$$

$$T_m = (\beta/2h\nu)(g_x^2 + g_z^2)/ [\sqrt{\{1 - (g_x^2/g_z^2)\}\{1 - (g_y^2/g_z^2)\}}] \quad (3)$$

This method allows the concentration to be determined by integration of "one dimension" (the g_z feature) of the absorption envelope as the size and shape of the absorption envelope are determined by its g values (which are known), concentration, and line shape. This method avoids integrating other features in the absorption envelope. For quantification of High g max EPR signals, the values of g_x and g_y have to be estimated. This is possible because as g_z approaches the theoretical limit of 4.0, g_x and g_y approach 0. The sum of their squared g values is therefore a maximum of 16 and as they are approaching axiality, g_x and g_y must be of similar magnitude (*29*).

Potentiometric Titration. Potentiometric titration of 110 μM NrfA in 50 mM Hepes, 2 mM $CaCl_2$, pH 7.0, was performed in the presence of dye mediators. The mediators (20 μM each) were potassium ferricyanide, 2,3,5,6-tetramethyl-*p*-phenylendiamine, 2,6-dichlorophenol indophenol, phenazine methosulfate, methylene blue, indigo carmine, anthroquinone 2,6-sulfonate, anthroquinone 2-sulfonate, phenosafranine, safranine O, benzyl viologen, and methyl viologen. To achieve stable potentials below −0.3 V, it was necessary to increase the methyl viologen concentration to 70 μM. Redox poise was achieved under the control of a potentiostat (Autolab electrochemical analyzer under the control of GPES software) using a three electrode cell configuration housed in an anaerobic chamber (N_2 atmosphere with O_2 < 2 ppm). Anaerobic samples were introduced into a freshly polished glassy carbon pot thermostated at 4 °C which constituted the working electrode. A platinum wire counter electrode was housed in a chamber separated from the NrfA sample by a Vycor Fritt and the Ag/AgCl, KCl (saturated) reference electrode (25 °C) contacted the sample through a Luggin capillary tip. Samples were poised at the desired potential with stirring until the current from the sample fell to zero indicating equilibration with the applied potential. After the zero current potential of the cell was confirmed to be the desired equilibration potential, the sample was then transferred to an EPR tube, sealed, and frozen within 1 min. Checks on the stability of the poised sample after removing potentiostatic control showed the potential drift was less than 5 mV over 5 min. Potentials are reported with reference to the standard hydrogen electrode (S.H.E.) by addition of 0.197 V to those measured.

Table 1: Data Collection and Refinement Statistics for *E. coli* NrfA[a]

data collection	
station	ID14.1 ESRF
wavelength/Å	0.934
resolution/Å	2.5
completeness/%	93.0 (94.6)
R_{sym}[b]/%	8.9 (24.4)
I/σ	5.4 (2.7)
independent reflections	71 769
total reflections	1 062 813
refinement	
resolution range/Å	20−2.5
reflections ($F > 0$)	69 831
refined structure	15 488 non-hydrogen atoms
R_{cryst}[c]/%	20.3 (28.0)
R_{free}[d]/%	24.3 (33.8)
RMS deviations	
bonds	C−N, 0.014 Å
	$N-C_\alpha$, 0.019 Å
	C_α−C, 0.021 Å
angles	$N-C_\alpha-C$, 2.00°
	$C-N-C_\alpha$, 1.80°
planes	peptides, 0.017 Å
	aromatics, 0.013 Å

[a] Figures in parentheses refer to data in the highest resolution bin. [b] $R_{sym} = \sum \sum |I\ i - \langle I \rangle| / \sum I\ i$ where $\langle I \rangle$ is the average of symmetry equivalent reflections and the summation extends over all observations for all unique reflections. [c] $R_{cryst} = \sum ||F_o| - |F_c|| / \sum |F_o|$ where F_o and F_c are the observed and calculated structure factors, respectively, and the summation extends over all unique reflections in the quoted resolution range. [d] For R_{free} (Brünger, 1992), the summation extends over a subset (5%) of reflections excluded from all stages of refinement.

RESULTS AND DISCUSSION

The 2.5 Å Crystal Structure of Escherichia coli Penta-Heme Cytochrome c Nitrite Reductase. The penta-heme cytochrome *c* nitrite reductase (NrfA) of *Escherichia coli* was crystallized in space group $P2_12_12_1$ with four monomers in the crystallographic asymmetric unit. The structure was solved by molecular replacement methods using the structure of the homologous enzyme from *Sulfurospirillum deleyianum* (7) and refined at 2.5 Å resolution to a final *R* factor of 20.3% (R_{free} = 24.3%) (Table 1). The crystal structure of NrfA is that of a homodimer formed from each monomer by transformation about a crystallographic 2-fold axis (Figure 1). This situation is analogous to that observed in the crystal structures of NrfA from both *S. deleyianum* and *W. succinogenes*, and in all three enzymes a key element of the dimer interface is the presence of a pair of long α-helices from each monomer which interacts across the dimer axis (*E. coli* contact area 1548 ± 21 Å^2). From a superposition of the structures from *E. coli* and *S. deleyianum*, an rms deviation of C_α atoms of 1.2 Å is obtained. This alignment gives a 46% identity over a total of 431 structurally equivalenced residues. This can be compared with an rms deviation of 0.9 Å between the aligned structures of the enzymes from *W. succinogenes* and *S. deleyianum* (77% identity over a total of 461 structurally equivalenced residues). The only significant nonaligned region of the structure involves residues 169−175, inclusive. This region forms an insertion in the *E. coli* enzyme sequence relative to that of *S. deleyianum*. A structurally aligned loop formed from residues 290 to 297 also differs in conformation between the two structures. For the same pair of enzymes, superposition of the hemes gives an rms deviation of 0.71 ± 0.01 Å.

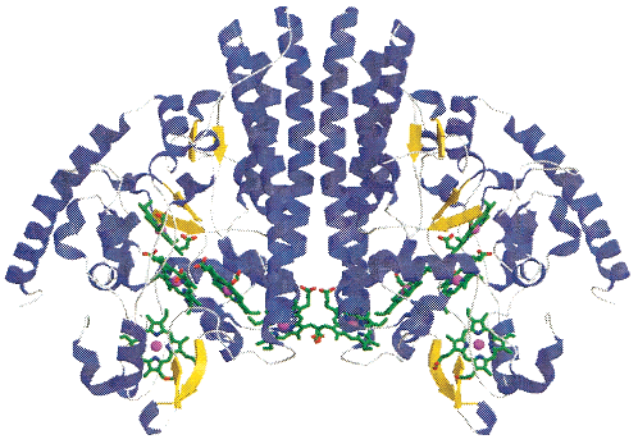

FIGURE 1: Overall structure of *E. coli* NrfA. A view of the NrfA dimer showing arrangement of monomers about a 2-fold crystallographic axis.

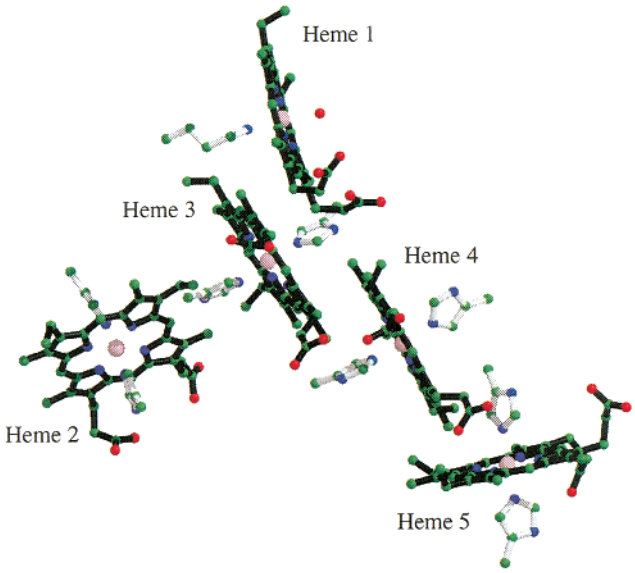

FIGURE 2: The arrangement of the heme groups plus histidine and lysine ligands in a NrfA monomer. The orientation of the hemes is similar to that shown in Figure 1. The hemes are numbered according to the order of attachment to CXXC motifs on the polypeptide chain.

All of the distinguishing features of the *W. succinogenes* and *S. deleyianum* cytochrome *c* nitrite reductases are apparent in *E. coli* NrfA. These include a catalytic heme with a lysine primary amine nitrogen as the proximal ligand, four electron-transferring bis-His ligated *c*-type hemes (Figure 2), a putative substrate inlet channel with positively charged electrostatic potential, and a putative product efflux channel that exhibits a more negative electrostatic potential. In addition, an active site calcium ion is conserved across all three structures both in terms of the identity of ligating residues and in the presence of two conserved water ligands (Figure 3). A further calcium-binding site was identified in a region of low sequence identity in the vicinity of heme 4. All of the key residues that provide for heme ligation are conserved in the three nitrite reductases. The properties of the hemes are summarized in Tables 2 and 3 and are compared with those of the *W. succinogenes* and *S. deleyianum* enzymes. The major differences arise from comparison of the interplanar angles of the histidine imidazole ligands (Table 3), where those observed in *E. coli* NrfA are smaller

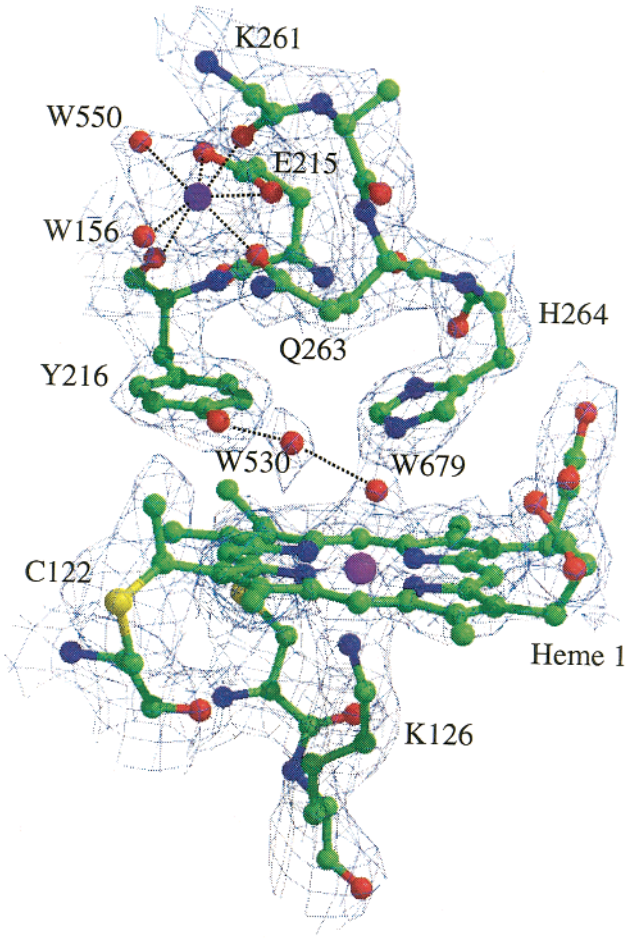

FIGURE 3: Detail of the NrfA active site showing the calcium ion and a bound water/hydroxide. Residues in the vicinity of the catalytic heme are shown along with (2Fo−Fc) electron density calculated at 2.5 Å resolution and contoured at 1.2 σ (where σ is the standard deviation of the map). The side-chain of lysine 261 has been removed for clarity. The hydrogen bonds linking the distal water (W679) to tyrosine 216 via a further, adjacent water molecule (W530) are shown as dotted lines as are the liganding interactions involving the neighboring calcium ion (shown in violet).

Table 2: Heme−Heme Distances and Angles of Cytochrome *c* Nitrite Reductases[a]

heme pair	plane angle/°			Fe−Fe distance/ Å			closest ring atom/ Å		
	Ec	Ws	Sd	Ec	Ws	Sd	Ec	Ws	Sd
2−3	75.8 ± 0.3	76.0	76.2 ± 0.7	12.6	12.5	12.8	6.3	6.0	6.2
1−3	25.0 ± 0.3	27.0	27.9 ± 0.5	9.7	9.7	9.6	4.3	4.3	4.4
1−4	17.9 ± 0.2	20.5	18.3 ± 0.7	16.5	16.5	16.6	8.3	8.4	8.5
4−5	72.5 ± 0.5	68.7	70.8 ± 1.0	11.3	11.2	11.2	5.8	5.6	5.7
3−4	8.5 ± 0.3	7.2	10.1 ± 1.1	9.4	9.4	9.3	4.5	4.0	3.8
5−5 (dimer)	87.1 ± 0.2	86.8	87.4 ± 0.6	11.9	11.7	11.8	5.8	5.9	5.7

[a] Data refer to Ec, *E. coli*; Ws, *W. succinogenes* [PDB code 1FS7]; and Sd, *S. deleyianum* [PDB code 1QDB]. Standard deviations are shown where applicable. No standard deviations are quoted for Fe−Fe distance and closest ring atom as they are less than 0.1 Å in each case.

than for the equivalent heme pair in the other two structures (the differences range from 6 to 17°). This is unlikely to be an effect of pH as the *S. deleyianum* and *E. coli* enzymes were both crystallized at pH 7.5, while the *W. succinogenes* enzyme was crystallized at pH 5.7.

Table 3: Properties of the Hemes of *E. coli* NrfA and *W. succinogenes* NrfA[a]

heme	ligands	His−His angle	solvent accessibility/Å^2
	E. coli		
heme 1	Lys126−OH^-/H_2O		28.3 ± 0.5
heme 2	His164−His301	21.2 ± 0.4	32.4 ± 1.1
heme 3	His94−His213	34.2 ± 2.0	11.3 ± 0.3
heme 4	His286−His393	64.4 ± 1.2	61.7 ± 1.2
heme 5	His275−His318	71.8 ± 1.7	76.6 ± 1.3
	W. succinogenes[b]		
heme 1	Lys134−OH^-/H_2O		29.3 (29.8 ± 0.8)
heme 2	His172−His313	27.4 (27.2 ± 0.7)	83.3 (93.8 ± 2.9)
heme 3	His102−His215	41.3 (46.1 ± 3.2)	17.5 (2.5 ± 0.5)
heme 4	His299−His405	81.1 (74.4 ± 2.4)	83.6 (68.2 ± 1.3)
heme 5	His288−His330	82.0 (87.9 ± 1.3)	70.9 (72.2 ± 5.4)

[a] Data for the *W. succinogenes* enzyme are taken from ref *8*. [b] For reference, data for the *S. deleyianum* enzyme (*7*) is given in brackets following that from *W. succinogenes*.

There is evidence in the 2Fo-Fc electron density maps for a distal ligand to the catalytic heme in each of the four copies of the NrfA monomer (Figure 3). We have interpreted this to be a water molecule in our model (W679), although an hydroxide ion is a possible alternative. The resulting mean Fe−O distance is 2.17 Å with a standard deviation of 0.04 Å. We have not restrained the position of this water molecule relative to the heme in the crystal structure refinement process. This can be compared with a distance of 2.05 Å observed in the structure of the enzyme from *W. succinogenes*. The difference in ligand distance is most likely due to the lower resolution of data used in our refinement. A nearby water molecule (W530 in Figure 3) is also conserved in the four molecules of the asymmetric unit of the *E. coli* enzyme. This water lies within hydrogen bonding distance of the liganding water and also hydrogen bonds to the phenolic hydroxyl of Tyr 216. Tyrosines in the vicinity of the active site have been postulated to deal with possible radical intermediates during the stepwise reduction of nitrite to ammonia by forming tyrosyl radicals during the catalytic cycle (*8*). Tyr 216 is adjacent to the tyrosine residue which was found to be partially ortho-hydroxylated in the *S. deleyianum* NrfA structure (*7*).

The solvent-accessible areas of the five hemes in each of the enzymes have been calculated for the crystal (and presumed solution) dimer structures and are shown in Table 3. For the *W. succinogenes* and *S. deleyianum* enzymes, hemes 2 and 4 show the largest solvent accessible area. Einsle et al (*8*) noted that the solvent-accessible region of heme 2 co-locates with a patch of strong positive electrostatic potential in both enzymes. They therefore identified this heme as the most likely entry point for electrons. In the *E. coli* dimer, on the other hand, the solvent-accessible area for heme 2 is only approximately half that of both hemes 4 and 5. However, inspection of the structure reveals the solvent-exposed edges of these hemes to lie in regions that are unlikely to be accessible to a donor protein of approximately 20 kDa molecular weight. Heme 4 lies at the base of a conical depression that is approximately 10 Å deep and 8 to 12 Å in diameter at the lip, while heme 5 lies in a V-shaped cavity at the edge of the dimer interface. The solvent-exposed edge of heme 2, however, lies on a relatively flat region of the molecular surface offering few restrictions

to donor protein access. The low solvent accessibility of heme 2 appears to arise, at least in part, from the formation of a salt bridge involving the side chain of Arg 201 with one of the heme propionate groups. This interaction is not observed in the structures of the other two enzymes as in both cases this arginine is substituted by a histidine residue, the shorter side chain of the latter precluding the formation of the ion pair.

The electropositive patch in the vicinity of heme 2 is conserved in the *E. coli* enzyme. As noted by Einsle et al (*8*), the strength of this patch correlates with the stability of the complexes of *W. succinogenes* and *S. deleyianum* NrfA enzymes with NrfH, their partner electron donor proteins. This conserved positive patch is significantly less pronounced in the *E. coli* enzyme than in the other two (Figure 4). The size of the positive patch is reduced in the *E. coli* NrfA structure by the substitution of an adjacent arginine residue (Arg 207 in *W. succinogenes* and Arg 206 in *S. deleyianum* enzymes) for a glutamine residue (Gln 205) in *E. coli*. Although weak, this represents one of the few positive surface patches apart from that at the site of substrate entry to heme 1. This weakness may relate to the observation that, unique among the three enzymes, it has not been possible to isolate the complex of *E. coli* NrfA with its electron donor, NrfB (data not shown).

If we accept heme 2 as the site of entry for electrons to the system, then given the difference in electron donor protein utilized by the *E. coli* enzyme, some differences in the shape of the molecular surface and charge distribution in the vicinity of the heme may be expected. From inspection of our structure, the seven residue insertion in the *E. coli* enzyme (residues 169 to 175) is seen to lie in this region and may well form part of the interaction surface with NrfB (Figure 4C). This, taken together with the generally more acidic nature of the electrostatic potential at the molecular surface in this region, may reflect the difference in electron donor. It is notable that this seven amino acid insertion is also present in NrfA from *Salmonella typhi* and *Haemophilus influenzae*, both of which also have a *nrfB*, rather than *nrfH* gene, in the *nrf* operon. Thus, this structural feature may prove to be a key difference between the NrfH- and NrfB-dependent subgroups of NrfA.

Optical Spectroscopy of Escherichia coli NrfA. The nature and geometry of heme ligands has characteristic effects on the spectroscopy of the cofactor. The oxidized and reduced UV/Vis spectra of NrfA (Figure 5A) are typical of *c*-type cytochromes. The oxidized spectrum has maxima at 409, 532, and 630 nm. The latter represents a ligand−metal charge transfer (LMCT) band of a high spin heme that has been observed for other cytochrome *c* nitrite reductases (*13*, *14*, *16*, *18*). The reduced NrfA spectrum exhibits the Soret, α, *β* bands at 420.5, 523.5, and 552 nm. In the UV/VIS MCD spectrum, intense low-spin ferric heme bands dominate over the wavelength range 300−600 nm (Figure 5B). In the Soret region (∼400 nm) of the MCD spectrum at room temperature, a single low spin heme gives rise to a derivative shaped band with a peak to trough intensity of approximately 150 M^{-1} cm^{-1} T^{-1} (*30*). The intensity of the MCD spectra presented in Figure 5B are therefore consistent with the presence of four low spin hemes as predicted from the crystal structure. The presence of low-spin ferric heme in NrfA is also supported by the α,*β*-MCD bands at 500−600 nm which are typical of low spin heme (*30*).

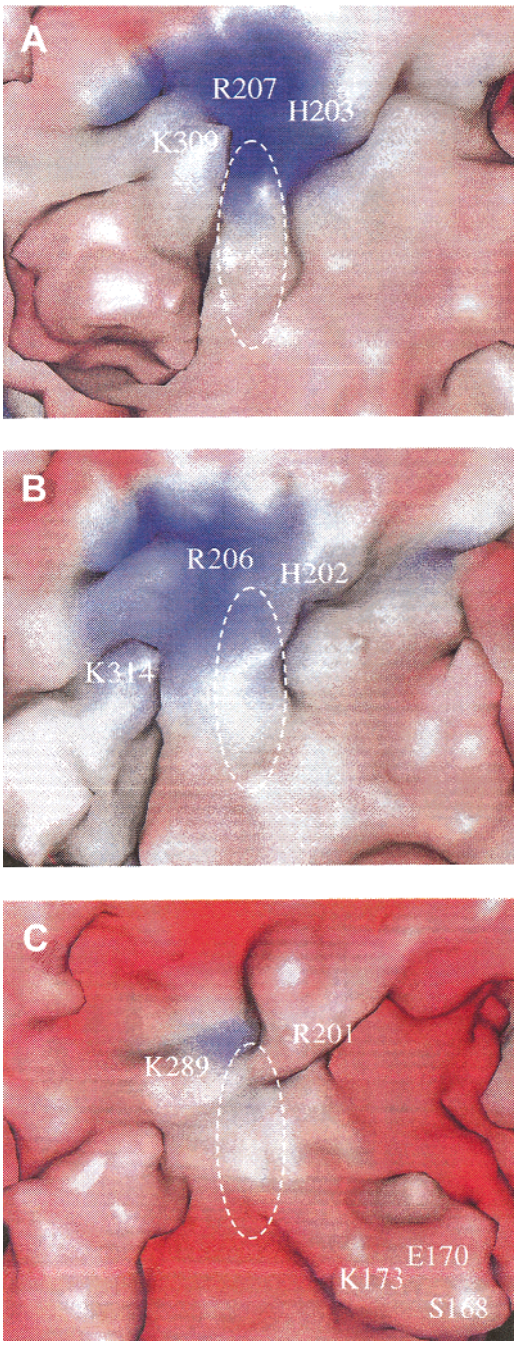

FIGURE 4: The conserved electropositive patch in the vicinity of heme 2. Views of the electrostatic potential color-coded (blue, basic; red, acidic) molecular surface of the NrfA dimer of *W. succinogenes* (A), *S. deleyianum* (B), and *E. coli* (C). The figure dimensions are approximately 20 × 20 $Å^2$, centered on heme 2 and arranged so that the view is into the vertically arranged, solvent-exposed heme edge. The approximate position of the heme edge is indicated by a dashed line. The positions of selected residues in the region of the conserved electropositive patch and of the seven residue insertion in the *E. coli* enzyme (residues 169 to 175) are indicated.

The charge-transfer band for low-spin ferric heme occurs in the near infrared (NIR) region of the electronic absorption spectrum (800−2500 nm). Although rarely detected by absorption spectroscopy, this band is readily observed by MCD spectroscopy, with the peak wavelength being an excellent indicator of the axial ligands to the heme iron (*30*). In NrfA, a broad positive LMCT band was observed at 1470

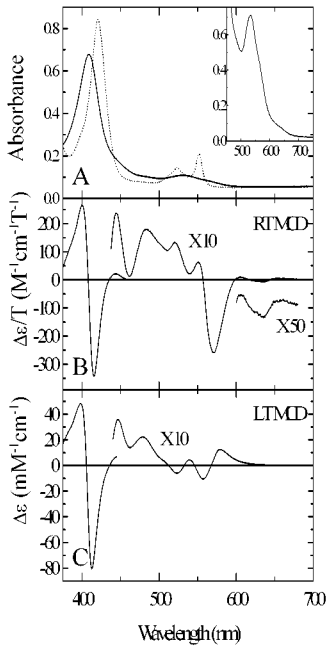

FIGURE 5: Spectroscopic properties of the NrfA in the UV/Vis region. (A) UV/Vis absorption spectra of oxidized (—) and sodium dithionite reduced (•••) NrfA. NrfA concentrations were 1.3 and 124 μM (insert) in 0.05 M Hepes, pH 7.0. (B) Room-temperature MCD spectrum of oxidized periplasmic NrfA. NrfA concentration was 124 μM in 0.05 M Hepes, pH* 7.0. (C) Low-temperature MCD spectrum of oxidized periplasmic NrfA. NrfA concentration was 124 μM in 0.05 M Hepes, pH* 7.0. Conditions used are as described in Experimental Procedures.

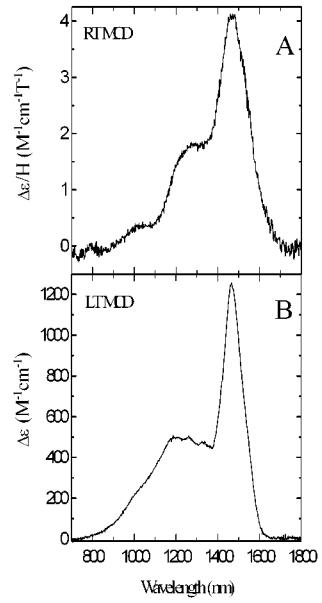

FIGURE 6: Spectroscopic properties of the oxidized NrfA in the near-IR region. (A) Room-temperature MCD spectrum. NrfA concentration was 62 μM in 0.05 M Hepes, pH* 7.0. (B) Low-temperature MCD spectrum. NrfA concentration was 62 μM in 0.05 M Hepes, pH* 7.0. Conditions used are as described in Experimental Procedures.

nm, with a vibrational sideband at lower wavelength (1200—1300 nm) (Figure 6A). This is characteristic of low spin bis-His coordinated ferric heme. The 1470 nm band displays a shoulder on its low energy side (ca. 1520 nm) which reflects the fact that four hemes in different protein environments contribute to this signal (Figure 6A). At the λ_{max}, low-spin bis-His heme NIR MCD bands characteristically have a $\Delta\epsilon$ of between 0.8 and 1.2 M^{-1} cm^{-1} T^{-1}. The intensity of the NrfA LMCT band (4 M^{-1} cm^{-1} T^{-1}) is thus consistent with four low spin hemes. This confirms that the crystal structure, which displays four bis-His coordinated hemes, reflects the room-temperature solution structure. At low temperature (4.2 K), the trough to peak intensity of the Soret band ($\Delta\epsilon$ = 125 mM^{-1} cm^{-1}) and the λ_{max} and intensity of the LMCT band (1470 nm, $\Delta\epsilon$ = 1.2 mM^{-1} cm^{-1}) are still consistent with four bis-His coordinated hemes suggesting that no gross changes have accompanied freezing of the NrfA to ultralow temperatures (Figure 5C and Figure 6B).

In the room temperature (RT) visible MCD (Figure 5B) and NIR MCD (Figure 6A) spectra of NrfA, negative features at 620 and 635 nm (Figure 5B), a positive band at 1000 nm, and a weak derivative at 800 nm were apparent. In general, the MCD spectra of high spin ferric heme contain a pair of high spin charge-transfer bands, both derivative in form, one in the region 600—670 nm and the second above 800 nm. The spectral features we have observed in NrfA arise from these bands (Figure 6A). These bands shift position with changes in axial ligation (*31*). Thus, histidine or lysine bound hemes with a water molecule bound in the distal pocket generally have a pair of bands in the regions 635—647 nm and 1050—1150 nm, respectively. If this water becomes deprotonated, these bands both shift to lower wavelengths to around 620 nm and 790—850 nm, respectively. If the water is removed completely the bands shift to higher wavelengths, 650—665 nm and above 1200 nm, respectively. Thus, taking the crystal structure into account we propose that the 620/800 nm and 635/1000 nm pairs of signals arise from the Lys-coordinated heme for which the oxygen observed as a sixth ligand is either hydroxide or water. The intensity of the 1000 nm band in the room-temperature NIR MCD spectrum (Figure 6A) suggests that a water ligand dominates at pH 7.

The intensity of MCD signals that arise from paramagnetic species increase with decreasing temperature. However, the features that arise from low spin ferric heme increase to a much greater extent (1 order of magnitude) than those which arise from high spin ferric heme. Consequently, the features at both 620/800 nm and 635/1000 nm are not detectable in the low temperature (LT) MCD spectra (Figure 5C and 6B) as they are swamped by the intensity of the low spin ferric heme signals.

The only previous reports of MCD spectra of NrfA are from the enzyme from *W. succinogenes* (*13*, *14*). The LT visible MCD spectrum was, like that of *E. coli* NrfA, dominated by low spin hemes with the peak-to-trough $\Delta\epsilon$ of the Soret band being ca. 115 mM^{-1} cm^{-1}. The LT NIR MCD spectrum exhibited a peak at 1510 nm ($\Delta\epsilon$ 1.2 mM^{-1} cm^{-1}), slightly red shifted as compared to that of the *E. coli* NrfA, but still of a wavelength and intensity consistent with four low spin bis-His ligated *c* hemes. The RT MCD of the *W. succinogenes* NrfA displayed a negative feature at 620 nm and a derivative centered at 850 nm that are characteristic of high spin heme. The 635 and 1000 nm features were much weaker. This suggests that the high spin heme in the *W. succinogenes* NrfA preparation was dominated by a Lys-$Fe^{(III)}$-OH^- form rather than the predominantly Lys-$Fe^{(III)}$-H_2O observed in the preparations of *E. coli* NrfA used in the present study.

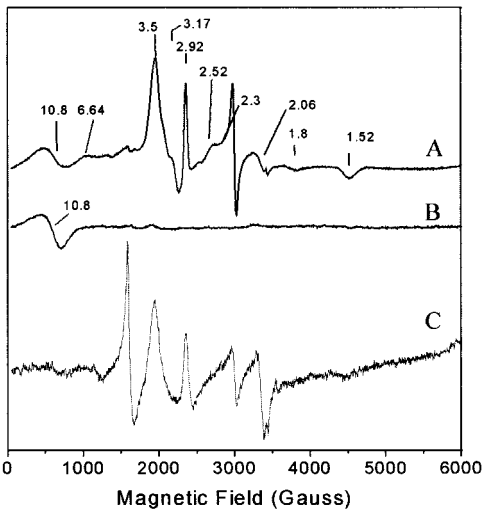

FIGURE 7: Perpendicular and parallel mode X-band EPR spectra of air-oxidized NrfA in frozen solution and in crystals. (A) Perpendicular mode spectrum of NrfA "as isolated". (B) Parallel mode spectrum of A. NrfA concentration was 69 μM in 0.05 M Hepes, pH 7.0. (C) Perpendicular mode spectrum of NrfA crystals. Spectra were collected at 10 K, 2 mW microwave power, 7.6 G modulation amplitude. The microwave frequency was 9.65 GHz for the perpendicular mode and 9.35 GHz for the parallel mode.

EPR Spectroscopy of Escherichia coli NrfA. The frozen solution perpendicular mode X-band EPR spectrum of air-oxidized NrfA is complex (Figure 7A). The prominent derivative features at $g \approx 3.5$ and $g = 10.8$ are atypical of the spin states of any magnetically isolated hemes. Parallel mode EPR spectroscopy shows only a derivative feature at $g \sim 10.8$ (Figure 7B). The presence of two derivative signals at g values $\sim$3−4 and 10−12, of which the latter is allowed in the parallel mode and the former is forbidden, are a pattern very similar to those observed from a weakly exchanged coupled high spin heme Fe(III) ($S = 5/2$) and Cu_B(II) ($S = 1/2$) in *E. coli* quinol oxidase (*32*). Thus, it is tempting to assign these features in NrfA to a weakly exchange coupled pair of paramagnets of $S = 5/2$ and $S = 1/2$. The clear candidate for the $S = 5/2$ species is the Lys-H_2O heme Fe(III). Identification of the $S = 1/2$ partner in the coupled pair is not unambiguous. One candidate is the bis-His coordinated heme 3 Fe(III) which lies at an edge−edge distance from heme 1 of 4.3 Å (Table 2). A heme pair with similar interplanar heme angles and edge−edge distances has been observed in the crystal structure of *Nitrosomonas europaea* cytochrome *c*554, a protein that can also exhibit similar EPR signals (*33*). However, we do not at this stage exclude the possibility that another $S = 1/2$ paramagnet, say from a radical species, may be a partner in the magnetically coupled pair.

The EPR signals at $g \approx 2.92$, 2.3, and 1.5 (Figure 7A) are typical for the g_z, g_y, g_x components of rhombic Fe(III) signals arising from low spin bis-His ligated Fe(III) hemes with near-parallel imidazole planes (*34*). Quantification of this signal by integration against a 1 mM copper EDTA standard gave an integer value of 1 mol spin per mol of enzyme. There are two hemes with near-parallel imidazole planes (hemes 2 and 3) (Figure 2, Tables 2 and 3). If heme 3 can been assigned to the exchanged coupled pair, then heme 2 is the most likely source of the $g \approx 2.92$, 2.3, and 1.5 signal. The remaining two low spin hemes, hemes 4 and 5, have near-perpendicular imidazole ligands (Figure 2, Table 3) and are expected, if magnetically isolated, to give rise to weak "Large g max" signals at around $g_z \approx 3.1-3.5$ (*34*). Such signals have low transition state probabilities with broad line widths. They may therefore be difficult to detect. The feature $g = 3.17$ (Figure 7A) may arise from one or both of these hemes.

Of the signals remaining in Figure 7A, that at $g \approx 6-6.5$ must arise from a magnetically isolated high spin ferric heme but corresponds to only a trace amount. Hence, it can originate from a small percentage of uncoupled high spin heme. The weak signals at $g = 2.52$ and $g = 1.8$ probably arise from low levels of low spin Lys-OH^- ligated heme, predicted to be present from the MCD, and may also arise from a small proportion of magnetically uncoupled heme. Both of these heme signals exhibited preparation to preparation variation. Weak signals at $g = 2.05$ are probably contributed to by a trace amount of Cu(II) and those between $g \approx 4.1-4.8$ most likely arise from adventitious Fe(III) and Fe-superoxide dismutase (Fe−SOD), which was a 5−10% contaminant in some preparations.

EPR spectra of redox centers are highly sensitive to the protein and solvent environment around the paramagnet. Thus, to assess whether the hemes in the NrfA crystals were in similar environments to those in the frozen solution the EPR spectrum of a collection of NrfA crystals in random orientation was acquired (Figure 7C). Although the spectral quality is not as high as that of frozen solution samples, the X-band perpendicular mode spectrum clearly shows many of the key features ascribed to heme Fe(III) in the frozen solution spectrum. The spectrum also has a large signal at $g = 4.3$ and $g \approx 2$ which most likely arises from iron (III) and copper (II) present in the crystallization liquor.

To gain insight into the redox properties of the NrfA hemes, EPR spectra of samples poised at defined potentials were measured. NrfA was poised using a potentiostat to avoid perturbation of heme coordination by dithionite (or breakdown products), that are known to bind to this class of enzyme (*14*). Spectra collected at +272 mV (not shown), +160 mV (not shown), +55 and 0 mV were essentially indistinguishable from each other (Figure 8A). Lowering the potential from 0 to −172 mV resulted in loss of the heme 2 rhombic low spin ferric heme signal ($g \approx 2.9$, 2.3, 1.5) (Figure 8A). This decrease in signal intensity could be fitted to a single component $n = 1$ Nernstian curve with $E_m = -37$ mV (Figure 8C). The signal intensity of the $g \approx 3.5$ and 10.8 features, arising from the magnetically coupled pair, decreased between −88 and −236 mV. This decrease fits well to an $n = 1$ Nernstian curve with $E_m = -107$ mV (Figure 8C). The derivative feature centered at $g = 10.8$ in the parallel mode EPR also decreased over the same potential range as the perpendicular mode $g = 3.5$ and $g = 10.8$ signals, consistent with it arising from the same coupled pair (Figure 8B and C). It should be noted that no new EPR features appeared concurrently with the decrease in intensity of the perpendicular mode $g = 3.5$ and $g = 10.8$ signal (Figure 8). If the two paramagnetic species contributing to this signal titrate as independent, near-iso-potential, $n = 1$ components, new $S = 5/2$ and $S = 1/2$ EPR signals are expected. For example, equilibration at the midpoint redox potential should yield an enzyme population where the spin states of the coupled pair are in the proportion 0.25[$S = 5/2$,

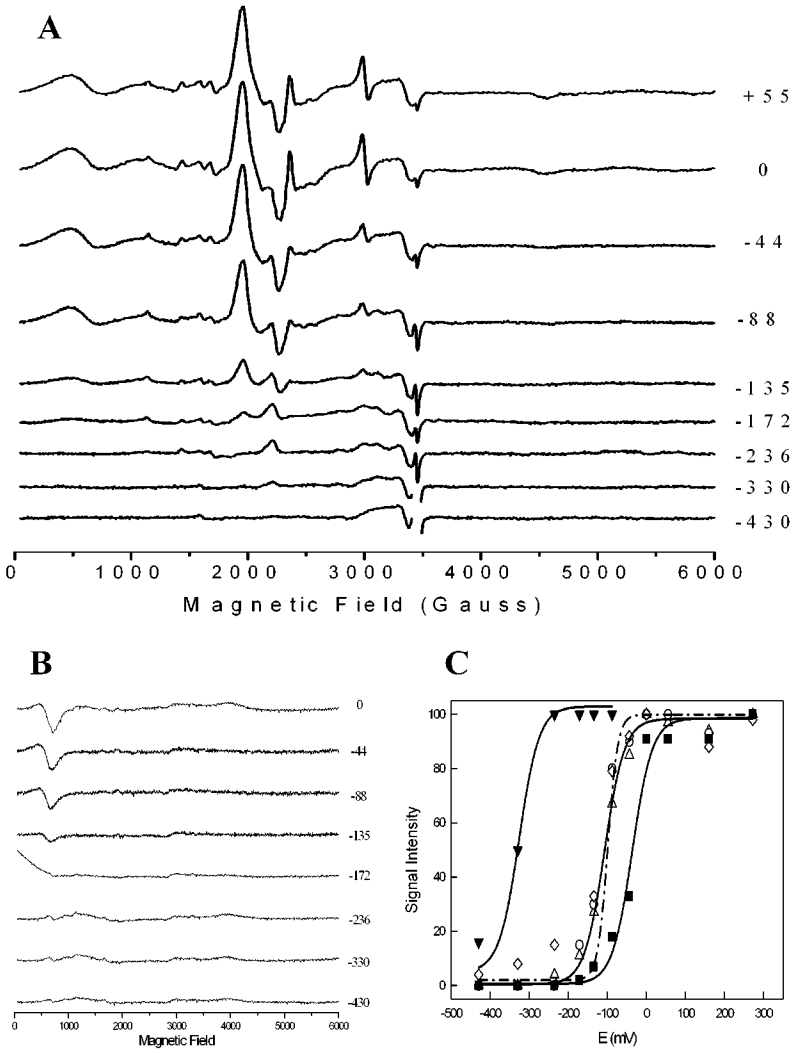

FIGURE 8: EPR spectra of electrochemically poised NrfA. (A) Perpendicular mode; (B) parallel mode; (C) plots of the EPR signals. ■, Plot of the peak to trough intensity of the $g = 2.3$ component of the low spin heme rhombic triplet. The solid line plotted through this symbol is an $n = 1$ Nernstian fit with E_m −37 mV. ○, △, ◇, Plot of the $g = 3.5$, $g = 10.8$, and parallel mode $g = 10.5$ signals arising from the magnetically coupled low spin−high spin heme pair. The solid line plotted through these symbols is an $n = 1$ Nernstian fit with E_m −107 mV to the $g = 3.5$ data. The dotted line is an $n = 2$ fit; ▼, Plot of the $g = 3.10$ "Large g max" signal. The solid line plotted through this symbol is an $n = 1$ Nernstian fit with E_m −323 mV.

$S = 1/2$]: 0.25[$S = 5/2$, $S = 0$]: 0.25[$S = 0$, $S = 1/2$]: 0.25-[$S = 0$, $S = 0$]. Thus, the [$S = 5/2$, $S = 0$] and [$S = 0$, $S = 1/2$] populations would be expected to give rise to EPR signals. The absence of any new $S = 5/2$ and $S = 1/2$ EPR signals is therefore puzzling, but could be explained if electron exchange between the two metals in the coupled pair was very rapid. It could be also explained if reduction of the coupled pair is a concerted two-electron process. Thus, the titration of the $g = 3.5$ and $g = 10.8$ signals has also been fitted with an $n = 2$ Nernstian curve (Figure 8C). This is clearly a less good fit of the data. Further study of this signal is required to explain this observation.

The "Large g max" feature at $g = 3.17$ is poorly resolved at potentials greater than −44 mV as a consequence of signal overlap with the $g = 3.5$ feature (Figure 8A). However, this signal can be clearly resolved when the $g = 3.5$ signal has decreased in intensity at potentials of less than −88 mV and titrates between −236 and −430 mV with a half peak intensity at around −323 mV (Figure 8A). Quantification of this weak signal gave an integer value of 1 mol spin per mol of enzyme. However, integration of such a weak signal is subject to uncertainty since the g_y and g_x features cannot be clearly resolved. Close inspection of the signal reveals that it is asymmetric and thus may represent two hemes with slightly different g_Z values. This would be consistent with the view that both hemes 4 and 5 with near-perpendicular imidazole planes contribute to this "Large g max" feature (Figure 2, Table 3). Alternatively, it is also possible that a magnetic interaction between the two low spin heme 5 across the NrfA dimer interface renders these hemes undetectable in the EPR. After titration, the samples were reoxidized and the EPR spectrum returned to the original form. The activity of the enzyme in spectrophotometric assays was unchanged after potential poising.

A visible absorption spectro-potentiometric study has previously been undertaken on the *E. coli* NrfA (*6*). The simplest interpretation of the titers was that there was one heme with an $E_m = +45$ mV, two with near isopotential $E_m = -90$ mV and two with near-isopotential $E_m = -210$ mV. The titer was, however, complex and other fits are possible including a combination of $n = 1$ and $n = 2$ components. Nevertheless, the spread of redox potentials over a ca. 300

mV span is similar to that observed in the present study even if the absolute potentials are somewhat higher. Dithionite was used as a reductant in the previous work, and it has been noted that dithionite reduction products can bind to the high spin heme of NrfA (*14*).

A number of EPR spectra have been published of cytochrome *c* nitrite reductases from different sources. The oxidized spectra of NrfA from *Desulfovibrio desulfuricans*, *S. deleyianum*, and *W. succinogenes* are broadly similar to that shown here for *E. coli* (*13*, *15*, *16*), exhibiting typical rhombic low spin ferric heme signal ($g \sim 2.9$, 2.3, and 1.5) and showing broad positive features at $g \sim 13.5$, 3.7 that can be assigned to an exchange coupled $S = 5/2$, $S = 1/2$ pair. However, a second set of signals at $g = 3.21$ and $g = 4.8$ that have been ascribed to an exchange coupled $S = 1/2$, $S = 1/2$ ferric heme pair in *W. succinogenes* are not apparent in the *E. coli* NrfA under the conditions addressed in the present study. Furthermore, since the $g = 4.8$ signal is absent in some published spectra of the *W. succinogenes* and *S. deleyianum* enzymes, it has been suggested that this signal only arises when the enzyme is complexed with a ca. 20 kDa cytochrome (*15*, *16*), most likely the tetra-heme redox partner, NrfH. The present analysis of the *E. coli* NrfA suggests rather that the $g = 3.21$ signal arises from a "Large g max" signal from hemes 4 and 5 in *W. succinogenes* and *S. deleyianum* NrfA.

Comparison of the redox properties of the hemes of the *E. coli* NrfA with those of the *W. succinogenes* and *S. deleyianum* NrfA is not possible because no equivalent data to those presented here for *E. coli* NrfA have yet been reported. However, an EPR-potentiometric study of *D. desulfuricans* NrfA has been reported (*35*). Although there is no structure available for this enzyme, it is very likely to be similar to that of *E. coli*, *W. succinogenes*, and *S. deleyianum* NrfA. Again, dithionite was used as a reductant in some of the experiments. Nevertheless, $g = 9.36$ and $g = 3.92$ signals that could arise from hemes 1 and 3 titrate between +200 and +20 mV, considerably higher than that reported in the present study. This is similar to a heme potential reported in the visible-potentiometric studies on *E. coli* NrfA (*6*) and could indicate the presence of a dithionite-derived distal ligand on heme 1. A rhombic signal ($g = 2.96$, 2.28, 1.50) that may arise from heme 2 titrates over the potential range of +7 to −55 mV and so would have an E_m comparable to that of the equivalent heme in *E. coli* NrfA. A signal at $g = 3.2$, which may arise from the hemes 4 and/or 5, is 50% reduced at −325 mV, suggesting that these hemes also have similar redox properties in both the *E. coli* and *D. desulfuricans* NrfA. An EPR-potentiometric study on the nitrite reductase of *Desulfovibrio vulgaris* has also been reported, but this is difficult to compare since as the study was on an enzyme complexed with a 20-kDa cytochrome redox partner (*18*), almost certainly the tetra-heme NrfH. Nevertheless, a rhombic signal at $g = 2.9$, 2.2, 1.5, which may arise from NrfA heme 2, and a signal $g = 3.6$, which could arise from the coupled pair, titrated over the range of +18 to −110 mV. A signal at $g = 3.16$, which might arise from NrfA hemes 4 and/or 5, appeared to be about 50% reduced at −290 mV. Thus, the redox potentials for NrfA hemes that can be tentatively derived from this study are broadly consistent with those of *E. coli* NrfA here.

In conclusion, the determination of the structure of *E. coli* NrfA has allowed a detailed magnetooptical-potentiometric study of the enzyme to be interpreted against a structural framework. This has enabled assignment of spectroscopic signals and redox potentials to some of the hemes. Using these data, it has also been possible to reevaluate previously published EPR studies on a range of cytochrome *c* nitrite reductases from other organisms, much of which was originally interpreted assuming six, rather than five, hemes. Finally, the study has presented the first structure of a NrfB-dependent, rather than NrfH-dependent, cytochrome *c* nitrite reductase. This has revealed distinct structural properties on the protein surface in the vicinity of heme 2, the putative electron input site, which may distinguish the two sub-groups of enzyme. The influence of the heme redox potentials, heme arrangement and redox partner on electron transfer and catalysis remains to be determined, but this study provides a framework around which this can now be addressed in *E. coli*.

ACKNOWLEDGMENT

We are grateful to Dr. Myles Cheesman and Dr. Vasily Oganesyan for discussion of the EPR of the coupled pair. We are also grateful to Dr. Andrew Leech for the SELDI analysis and to Ann Reilly, Jeremy Thornton, and David Clarke for technical assistance.

REFERENCES

1. Potter, L. C., Millington, P., Griffiths, L., Thomas, G. H., and Cole, J. A. (1999) *Biochem. J. 344 Pt 1*, 77−84.
2. Tyson, K. L., Cole, J. A., and Busby, S. J. (1994) *Mol. Microbiol. 13*, 1045−55.
3. Berks, B. C., Ferguson, S. J., Moir, J. W., and Richardson, D. J. (1995) *Biochim. Biophys. Acta 1232*, 97−173.
4. Kajie, S., and Anraku, Y. (1986) *Eur. J. Biochem. 154*, 457−463.
5. Hussain, H., Grove, J., Griffiths, L., Busby, S., and Cole, J. (1994) *Mol. Microbiol. 12*, 153−63.
6. Eaves, D. J., Grove, J., Staudenmann, W., James, P., Poole, R. K., White, S. A., Griffiths, I., and Cole, J. A. (1998) *Mol. Microbiol. 28*, 205−16.
7. Einsle, O., Messerschmidt, A., Stach, P., Bourenkov, G. P., Bartunik, H. D., Huber, R., and Kroneck, P. M. (1999) *Nature 400*, 476−80.
8. Einsle, O., Stach, P., Messerschmidt, A., Simon, J., Kroger, A., Huber, R., and Kroneck, P. M. (2000) *J. Biol. Chem. 275*, 39608−16.
9. Igarashi, N., Moriyama, H., Fujiwara, T., Fukumori, Y., and Tanaka, N. (1997) *Nat. Struct. Biol. 4*, 276−84.
10. Iverson, T. M., Arciero, D. M., Hsu, B. T., Logan, M. S., Hooper, A. B., and Rees, D. C. (1998) *Nat. Struct. Biol. 5*, 1005−12.
11. Bamford, V., Dobbin, P. S., Richardson, D. J., and Hemmings, A. M. (1999) *Nat. Struct. Biol. 6*, 1104−7.
12. Taylor, P., Pealing, S. L., Reid, G. A., Chapman, S. K., and Walkinshaw, M. D. (1999) *Nat. Struct. Biol. 6*, 1108−12.
13. Blackmore, R. S., Brittain, T., Gadsby, P. M., Greenwood, C., and Thomson, A. J. (1987) *FEBS Lett. 219*, 244−8.
14. Blackmore, R. S., Gadsby, P. M., Greenwood, C., and Thomson, A. J. (1990) *FEBS Lett. 264*, 257−62.
15. Liu, M. C., Liu, M. Y., Payne, W. J., Peck, H. D., Jr., Le Gall, J., and DerVartanian, D. V. (1987) *FEBS. Lett. 218*, 227−30.
16. Schumacher, W., Hole, U., and Kroneck, P. M. (1994) *Biochem. Biophys. Res. Commun. 205*, 911−6.
17. Stach, P., Einsle, O., Schumacher, W., Kurun, E., and Kroneck, P. M. (2000) *J. Inorg. Biochem. 79*, 381−5.

18. Pereira, I. A. C., LeGall, J., Xavier, A. V., and Teixeira, M. (2000) *Biochim. Biophys. Acta 1481*, 119−30.
19. Roldan, M. D., Sears, H. J., Cheesman, M. R., Ferguson, S. J., Thomson, A. J., Berks, B. C., and Richardson, D. J. (1998) *J. Biol. Chem. 273*, 28785−90.
20. Simon, J., Gross, R., Einsle, O., Kroneck, P. M., Kroger, A., and Klimmek, O. (2000) *Mol. Microbiol. 35*, 686−96.
21. Potter, L. C., and Cole, J. A. (1999) *Biochem. J. 344 Pt 1*, 69−76.
22. Otwinowski, Z., and Minor, W. (1997) *Methods Enzymol. 276*, 307−26.
23. Bailey, S. (1994) *Acta Crystallogr. D50*, 760−63.
24. Jones, T. A., Zou, J. Y., Cowan, S. W., and Kjeldgaard, M. (1991) *Acta Crystallogr. A 47*, 110−9.
25. Brunger, A. T. (1992) *Nature 355*, 472−75.
26. Laskowski, R. A., Macarthur, M. W., Moss, D. S., and Thornton, J. M. (1993) *J. Appl. Crystallogr. 26*, 283−91.
27. Holm, L., and Sander, C. (1993) *J. Mol. Biol. 233*, 123−38.
28. Christopher, J. A. (1997) Center for Macromolecular Design, Texas A&M University, College Station TX 77843-2128.
29. Aasa, R., and Vangaard, T. (1975) *J. Magn. Reson. 19*, 308−15.
30. Thomson, A. J., Cheesman, M. R., and George, S. J. (1993) *Methods Enzymol. 226*, 199−232.
31. Cheesman, M. R., Watmough, N. J., Gennis, R. B., Greenwood, C., and Thomson, A. J. (1994) *Eur. J. Biochem. 219*, 595−602.
32. Oganesyan, V., Butler, C., Watmough, N., Thomson, A., and Cheesman, M. (1998) *J. Am. Chem. Soc. 120*, 4232−4233.
33. Andersson, K. K., Lipscomb, J. D., Valentine, M., Munck, E., and Hooper, A. B. (1986) *J. Biol. Chem. 261*, 1126−38.
34. More, C., Belle, V., Asso, M., Fournel, A., Roger, G., Guigliarelli, B., and Bertrand, P. (1999) *Biospectroscopy 5*, S3−18.
35. Costa, C., Moura, J. J., Moura, I., Liu, M. Y., Peck, H. D., Jr., LeGall, J., Wang, Y. N., and Huynh, B. H. (1990) *J. Biol. Chem. 265*, 14382−8.

BI015765D